Hindawi Publishing Corporation
International Journal of Photoenergy
Volume 2015, Article ID 230808, 11 pages
http://dx.doi.org/10.1155/2015/230808

Research Article

Enhanced Photoreduction Activity of Carbon Dioxide over Co_3O_4/CeO_2 Catalysts under Visible Light Irradiation

Ying Huang,[1,2] Chang-Feng Yan,[1,2] Chang-Qing Guo,[1] and Shi-Lin Huang[1]

[1]*Guangzhou Institute of Energy Conversion, Chinese Academy of Sciences, Guangdong 510640, China*
[2]*University of Chinese Academy of Sciences, Beijing 100039, China*

Correspondence should be addressed to Chang-Feng Yan; yancf@ms.giec.ac.cn

Received 10 December 2014; Revised 31 March 2015; Accepted 16 April 2015

Academic Editor: Franca Morazzoni

A series of new two semiconductor catalysts, Co_3O_4/CeO_2, were prepared by glycine-nitrate combustion method for photocatalytic reduction of carbon dioxide to produce methanol and ethanol under visible light ($\lambda > 400$ nm) irradiation. The catalysts were characterized by BET, UV-vis spectra, XRD, SEM, PL, and XPS and the results indicated that the catalyst with 5 wt.% of Co_3O_4 has the highest yield among all kinds of tests with the methanol yield of 1.52 μmol·g^{-1}·h^{-1} and the ethanol yield of 4.75 μmol·g^{-1}·h^{-1}, which are about 2.34 and 1.71 times as large as those of CeO_2. However, methanol and ethanol can hardly be detected for Co_3O_4 under the same condition because of its too narrow band gap. The improvement of the photoreduction activity of Co_3O_4 doped CeO_2 was caused by the separation of electron-hole pairs of Co_3O_4/CeO_2 and charge transfer between Co_3O_4 and CeO_2, mimicking the Z-scheme in photosynthesis.

1. Introduction

Carbon dioxide, one of the major greenhouse gases which is largely formed by fossil fuels consumption, can be conversed back to fuel with water or hydrogen by thermochemical or photocatalytic approach [1]. Photocatalytic reduction of carbon dioxide to methanol or other organic fuels, which is a process to both reduce carbon dioxide emissions and resolve energy crisis, has been proved to be a prospective way to convert solar energy by using semiconductor catalysts, like TiO_2 [2–4], CdS [5], SiC [6], g-C_3N_4 [7, 8], and graphene oxide [9, 10]. Due to shortages of narrow band gap of single semiconductor catalyst, two-semiconductor ones such as Co_3O_4/CeO_2 are expected to be explored in order to improve photocatalytic properties and to widen the responsive wavelength range for visible light, thus enhancing the total efficiency of photocatalysis.

Among various semiconductor photocatalysts, CeO_2 has some properties similar to titania catalyst such as wide band gap, nontoxicity, and high stability [11]. However, the main light absorption region of CeO_2 lies in the near ultraviolet and its low quantum efficiency and high recombination rate of electrons holes also constrain its development [12]. Due to the special f and d electron orbital structure of cerium atom, some metal oxide semiconductors like TiO_2 [13], Bi_2O_3 [14], and Cu_2O [11] can be easily doped with pure CeO_2 to enhance visible light absorption and quantum efficiency. Cobalt-based catalysts have been recently reported as photocatalysts for water oxidation [15–18], hydrogen production [19], and organic pollutants degradation [20–22]. Co is significantly less abundant than other transition metals like Fe, Mn, and Ni, but it is emerging as a potential metal for catalytic processes because of its light harvesting and electron mediating properties [19]. Cobalt oxides, for example, CoO and Co_3O_4, are p-type semiconductors with interesting electronic and magnetic properties [23]. The p-n heterojunction semiconductor structure combined with cobalt oxide and other n-type semiconductors such as $BiVO_4$ [23] or WO_3 [20] has been investigated as an effective way to improve the photocatalytic activities under visible light irradiation. In this case, CeO_2 as an n-type semiconductor with wide band gap may possibly bring out a similar heterojunction structure with Co_3O_4 to enhance the efficiency of visible light absorption by shortening the band gap, in which such p-n

heterojunction structure can hardly work to reduce carbon dioxide according to the band theory because the conduction band potential of Co_3O_4 is too positive to start the reduction. However, CeO_2 is also a good reducing agent because of its relatively more negative reductive potential (around −0.5 eV) and Co_3O_4 doped CeO_2 with shorter band gap (2.07 eV) can act as a good cocatalyst, sensitizer, and oxidation agent of the composite with high positive potential (+2.44 eV) in the Z-scheme reaction mimicking photosynthesis. Recent studies on Z-scheme without mediators or so-called direct Z-scheme were carried out to explain charge separation at the interface between two semiconductors in a hybrid photocatalyst [24–27]. Further application of Co_3O_4/CeO_2 photocatalytic reduction of carbon dioxide to methanol and ethanol in the Z-scheme model has not been reported, which could enhance photocatalytic activity.

In this paper, a series of Co_3O_4/CeO_2 catalysts were prepared by glycine-nitrate combustion method for photocatalytic reduction of carbon dioxide to methanol and ethanol under visible light ($\lambda > 400$ nm) irradiation. The structures of catalysts were characterized by XRD, UV-vis absorption spectra, BET analysis, and SEM testing. And a series of measurements, such as XPS and PL, were carried out for the mechanism of improvement of the photoreduction activity of Co_3O_4 doped CeO_2.

2. Experimental

2.1. Preparation of Co_3O_4/CeO_2 Catalysts. The $Co(NO_3)_2 \cdot 6H_2O$ and $Ce(NO_3)_3 \cdot 6H_2O$ were mixed in the appropriate molar ratios with a minimum volume of distilled water to form a transparent solution. Then the glycine solution was slowly dropped to the metal nitrate aqueous solution during stirring. The glycine to nitrate ratio was set to 0.3 as the literature described [28]. The resulting solution was then kept stirring for an hour in order to gain transparent sol. Afterwards, the crucible was dried at 75°C in an oven for more than six hours until a transparent moisture-sensitive glassy material was obtained. This glassy material with fine mesh was heated in a muffle furnace up to around 180°C, and then it generated spontaneous combustion with large amounts of gases evolution and a foamy voluminous powder. Then the powder was calcined at 300°C or 400°C or 500°C or 600°C for an hour to burn off any carbonaceous residues in the catalyst. In addition, CeO_2 was prepared by the same method without adding $Co(NO_3)_2 \cdot 6H_2O$.

2.2. Catalyst Characterization. Specific surface area, average pore diameter, total pore volume, and pore size distribution of the samples were determined from the adsorption and desorption isotherms of nitrogen at 77 K after outgassing procedure under vacuum at 250°C for 10 h, using a Quantachrome Autosorb-1 instrument. X-ray diffraction (XRD) analysis was performed with the PANalytical X'Pert diffractometer (X'Pert PRO MPD, PW3040/60) within the 2-θ ranging from 5° to 80° by a speed of 6° per minute with Cu-Kα ($\lambda = 0.154060$ nm) radiation (40 kV, 40 mA). The crystallite size was calculated by the Scherrer equation from the XRD spectra. The surface morphology was observed by the field emission-scanning electron microscope (FE-SEM, S-4800). UV-vis spectroscopy in the 300 nm–1000 nm was measured with a Lambda 750 Diffuse Reflectance Spectroscopy. X-ray photoelectron spectroscopy (XPS) analysis was conducted on a thermo ESCALAB 250XI multifunctional imaging electron spectrometer (Thermo Fisher Scientific Inc.) equipped with an Al Kα radiation source. Fluorescence spectra were obtained using a photoluminescence (PL) spectrometer (Perkin Elmer, LS-55). The concentration of methanol and ethanol was detected by a gas chromatograph (GC-7890II), equipped a flame ionization detector and a stainless steel packed column (PorapakQ, 2 mm × 1 m).

2.3. Photocatalytic Reaction Testing. The photocatalytic reaction was performed in a continuous-flow reactor system as shown in Figure 1. A 300W Xe lamp located in the center of the quartz cool trap was the light source and the UV light wavelength below 400 nm was filtered by a 2.0 M sodium nitrite solution layer between light source and reacting liquid [4]. Prior to experiment, sodium carbonate (3.18 g) and sodium sulfite (3.78 g) were dissolved in 300 mL deionized water. In this paper, sodium sulfite and sodium sulfide play a role as the sacrifice agent to scavenge photogenerated holes. Then the solution was injected into the reactor. Before irradiation, ultrapure carbon dioxide was bubbled through the solution in the reactor for at least 30 minutes to ensure that all dissolved oxygen was eliminated while adsorption and desorption of carbon dioxide in the solution and on the photocatalyst reached the equilibrium. 300 mg of catalyst powder was then added into above solution in the reactor for a five-hour irradiation. The solution of about 1 mL in the reactor was withdrawn as a sample each hour.

3. Results and Discussion

3.1. Characterization of Samples with Different Cobalt Loading. Figure 2 shows the X-ray diffraction patterns of Co_3O_4/CeO_2 photocatalysts prepared by glycine-nitride combustion method and calcined at 400°C, along with CeO_2 and Co_3O_4 which were prepared at the same conditions. Diffraction peaks corresponding to the hexagonal phases of CeO_2 are present for all Co_3O_4/CeO_2 photocatalysts with different mass faction of Co_3O_4 loading. Six main reflections belong to a typical fcc fluorite structure of CeO_2 (ICSD-169029), corresponding, respectively, to the [111], [200], [220], [311], [222], and [400] planes. And ten main reflections belong to Co_3O_4 (ICSD-069366) as shown in Figure 2. With the increase of the Co_3O_4 from 1 wt.% to 20 wt.%, the diffraction peaks of CeO_2 become weaker, which indicates a continuous decrease in the crystallization degree of CeO_2. The diffraction peaks of Co_3O_4 are hard to be detected in all Co_3O_4/CeO_2 catalysts. The reasons why the strong Co oxides peaks absence had been discussed in our previous work [29], which may be attributed to (1) highly dispersed Co_3O_4 on the surface of ceria, (2) the formation of Co-Ce-O solid solution, or (3) a combination of two points stated above. However, some weak diffraction peaks for Co_3O_4 can still be noted, which suggests the existence of Co_3O_4 on the surface of particles. Either high dispersion of Co_3O_4 on the surface

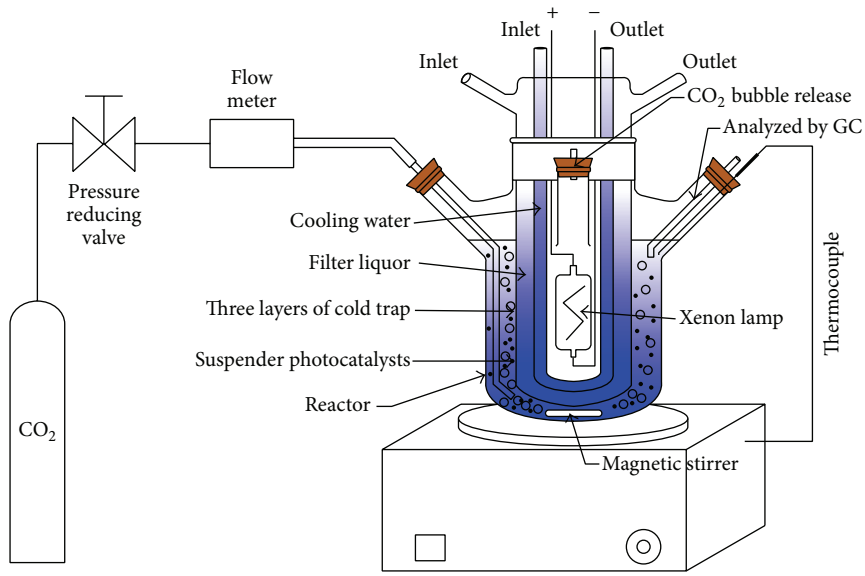

FIGURE 1: Schematic view of reactor system for photocatalytic reduction of carbon dioxide.

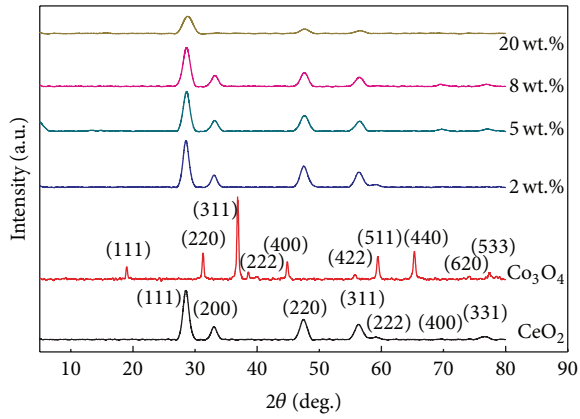

FIGURE 2: XRD pattern of Co_3O_4/CeO_2 photocatalysts with different mass faction of Co_3O_4 doping.

of CeO_2 or formation of Co-Ce-O solid solution indicates CeO_2 doped with Co_3O_4 instead of mixed oxides formed.

The UV-vis spectra of the catalysts are shown in Figure 3. The light absorption of all catalysts covers the visible region. The band gap of CeO_2 is estimated to be 2.93 eV from the plot of the $(\alpha h\nu)^2$ versus photon energy $(h\nu)$ [4, 6] as shown in the inset of Figure 3(a), which is 0.27 eV narrower than that of the commercial CeO_2 with the band gap of 3.2 eV. It has been reported that CeO_2, as an n-type semiconductor, has band gap varying from 2.7 to 3.4 eV depending on the preparation method [30]. The red shift of the CeO_2 sample might be attributed to trivalent ionic cerium compounds. Similarly, the band gap of Co_3O_4 is estimated to be 2.0 eV, which is matched with the reported band gap (2.07 eV) [20]. In contrast to CeO_2, the Co_3O_4/CeO_2 have strong absorption in the visible region ($\lambda > 400$ nm) and the visible light absorbance increases along with the addition of Co_3O_4 (Figure 3(c)).

In order to investigate the electronic environment and oxidation state of the CeO_2 sample, XPS analysis was performed. Eight peaks for Ce 3d of CeO_2 sample are shown in Figure 4(a), which are different from those of the reported CeO_2 with six peaks at binding energies 882.5, 888.7, 898.2, 900.7, 907.6, and 916.5 (±0.2) eV [31, 32]. Other authors have proved that the shape of Ce 3d peaks changes after normalizing the intensity of Ce 3d peaks for Ce_2O_3 and CeO_2 [32] when Ce_2O_3 is mixed or doped with CeO_2. And the peaks can be divided into more than six peaks, which may be attributed to the presence of Ce^{3+} [33]. Among all of these ten peaks in Figure 4(a), v, v'', v''', u, u'', and u''' are attributed to the presence of Ce(IV), and v_0, v', u_0, and u' are attributed to the presence of Ce(III) [34]. Three peaks for O 1s of CeO_2 sample are shown in Figure 4(b). Two peaks at 529.7 and 531.3 eV are attributed to O-Ce(IV) bond and O-Ce(III) bond, respectively [34], which indicates the existence of both CeO_2 and Ce_2O_3 [35]. In this case, Ce_2O_3 with much shorter band gap of 2.4 eV can shorten the band gap of CeO_2 and enhance the visible light absorption, which is in line with the UV-vis spectra.

Table 1 displays the specific surface area, the pore volume, the total pore volume of pure CeO_2 and Co_3O_4, and the catalysts with Co_3O_4 loading of 2 wt.%, 5 wt.%, and 8 wt.%. As the Co_3O_4 loading increases from 0 wt.% to 100 wt.%, the surface areas decrease from 100.14 to 24.47 m^2/g, and the total pore volume decreases as well. It can be attributed to the mutual filling of the pore structure during the forming of Co_3O_4 and CeO_2 which can be proved by the pore diameter distribution in Figure 5. And pore size distribution of Co_3O_4/CeO_2 catalysts that smaller than 10 nm decreases sharply compared to that of Co_3O_4 or CeO_2 and mainly is distributed in mesopore region from 10 to 50 nm. When

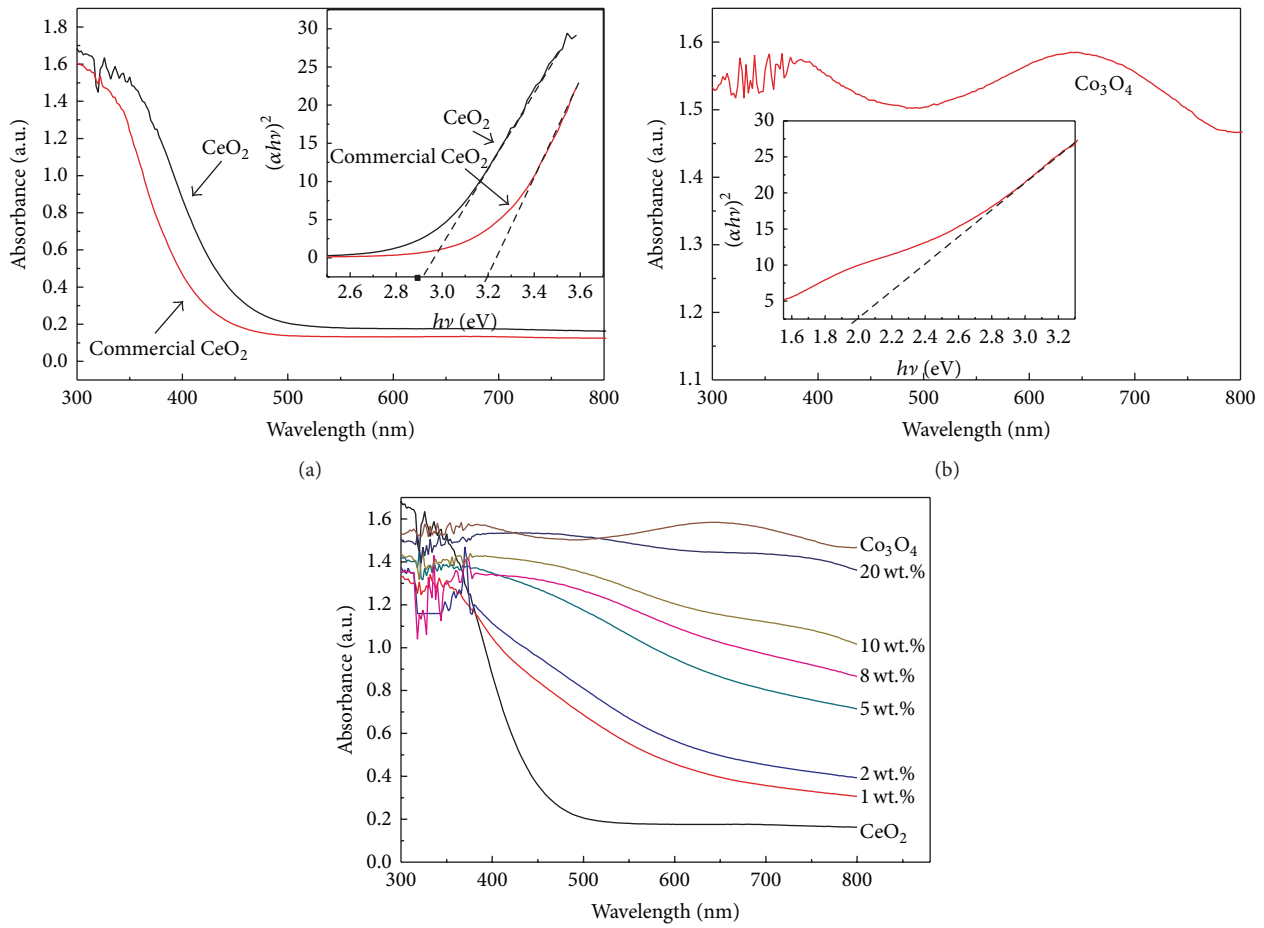

Figure 3: UV-vis absorption spectra of CeO_2 and commercial CeO_2 catalyst (a), Co_3O_4 (b), and the Co_3O_4/CeO_2 photocatalysts (c).

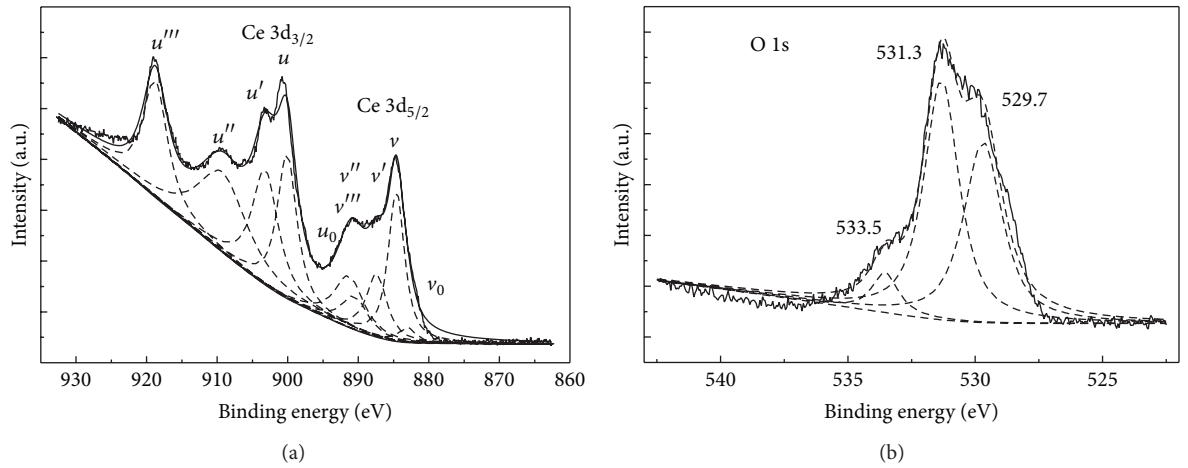

Figure 4: XPS spectra of the Ce 3d region (a) and the O 1s region (b) for the CeO_2 sample.

the Co_3O_4 loading increased from 2 wt.% to 8 wt.%, there is no distinct difference in specific surface area, average pore diameter, and total pore volume, which indicates that addition of Co_3O_4 in the Co_3O_4 loading range has little effect on the corresponding structure of Co_3O_4/CeO_2 catalysts. The sample with 5 wt.% Co_3O_4 loading has biggest specific surface area and uniform pore diameter distribution among all the tested Co_3O_4/CeO_2 catalysts. In addition, larger specific surface area, smaller pore volume, and total pore volume compared to those of commercial CeO_2 suggest that

Table 1: Characteristic of Co_3O_4/CeO_2 catalysts with different mass fraction of Co_3O_4.

Catalyst mass fraction of Co_3O_4 doping (%)	BET surface area (m^2/g)	Average pore diameter (nm)	Total pore volume (cm^3g^{-1})
0 (CeO_2)	100.14	4.68	0.12
0 (commercial CeO_2)	71.41	15.22	0.27
2.0	34.69	11.41	0.11
5.0	38.28	10.19	0.10
8.0	33.20	11.65	0.10
100 (Co_3O_4)	25.47	13.28	0.08

Table 2: Mean methanol and ethanol yield on Co_3O_4/CeO_2 catalysts under visible light irradiation ($\lambda > 400$ nm).

Catalyst mass fraction of Co_3O_4 doping (%)	Mean yield of methanol $\mu mol \cdot h^{-1} g_{cat}^{-1}$	Mean yield of ethanol $\mu mol \cdot h^{-1} g_{cat}^{-1}$
0 (CeO_2)[a]	0.68	2.77
1.0[a]	1.51	2.87
2.0[a]	1.5	3.95
8.0[a]	1.22	3.15
10.0[a]	1.18	2.43
100 (Co_3O_4)[a]	0	0
5.0[a]	1.52	4.75
5.0[b]	0.91	2.22
5.0[c]	0.75	2.16

0.30 g catalysts reacted in 300 mL solution of (a) 0.1 M NaOH + 0.1 M Na_2SO_3, (b) 0.1 M Na_2CO_3 + 0.1 M Na_2S, and (c) 0.1 M Na_2CO_3 + 0.1 M Na_2SO_3. A 300 W Xenon lamp ($\lambda > 400$ nm) irradiated for 5 hours.

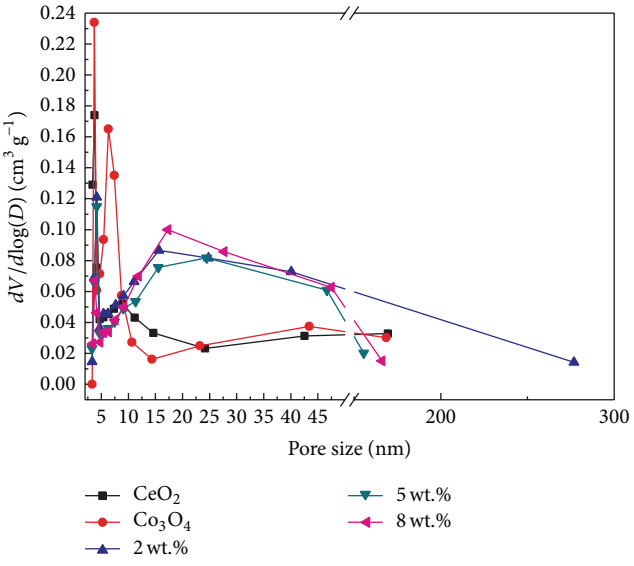

Figure 5: Pore diameter distribution of catalysts with different mass faction of Co_3O_4 doping.

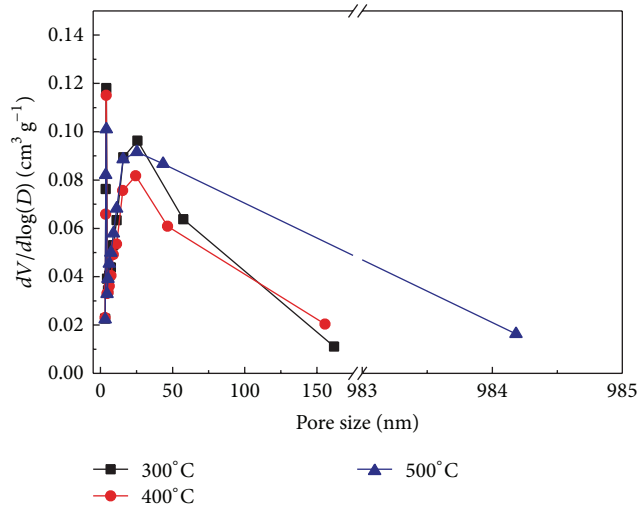

Figure 6: Pore diameter distribution of catalysts under different calcination temperature.

CeO_2 prepared by glycine-nitrate combustion method is a more potential carrier for catalysis.

The average methanol and ethanol yields, denoted as the average production rate of methanol and ethanol for each hour over the photocatalysts, are shown in Table 2. The photocatalytic activity of CeO_2 can be well improved via loading Co_3O_4 on CeO_2 by glycine-nitrate combustion method. No methanol and ethanol conversion was detected for Co_3O_4 catalyst under visible light irradiation because of its conduction band maximum being too positive to reduce carbon dioxide to methanol or ethanol. The sample with 5 wt.% Co_3O_4 has the best performance to produce both methanol and ethanol, which can be attributed to its better specific surface area, the proper pore volume, and pore size (Table 1). Increasing the Co_3O_4 loading from 0

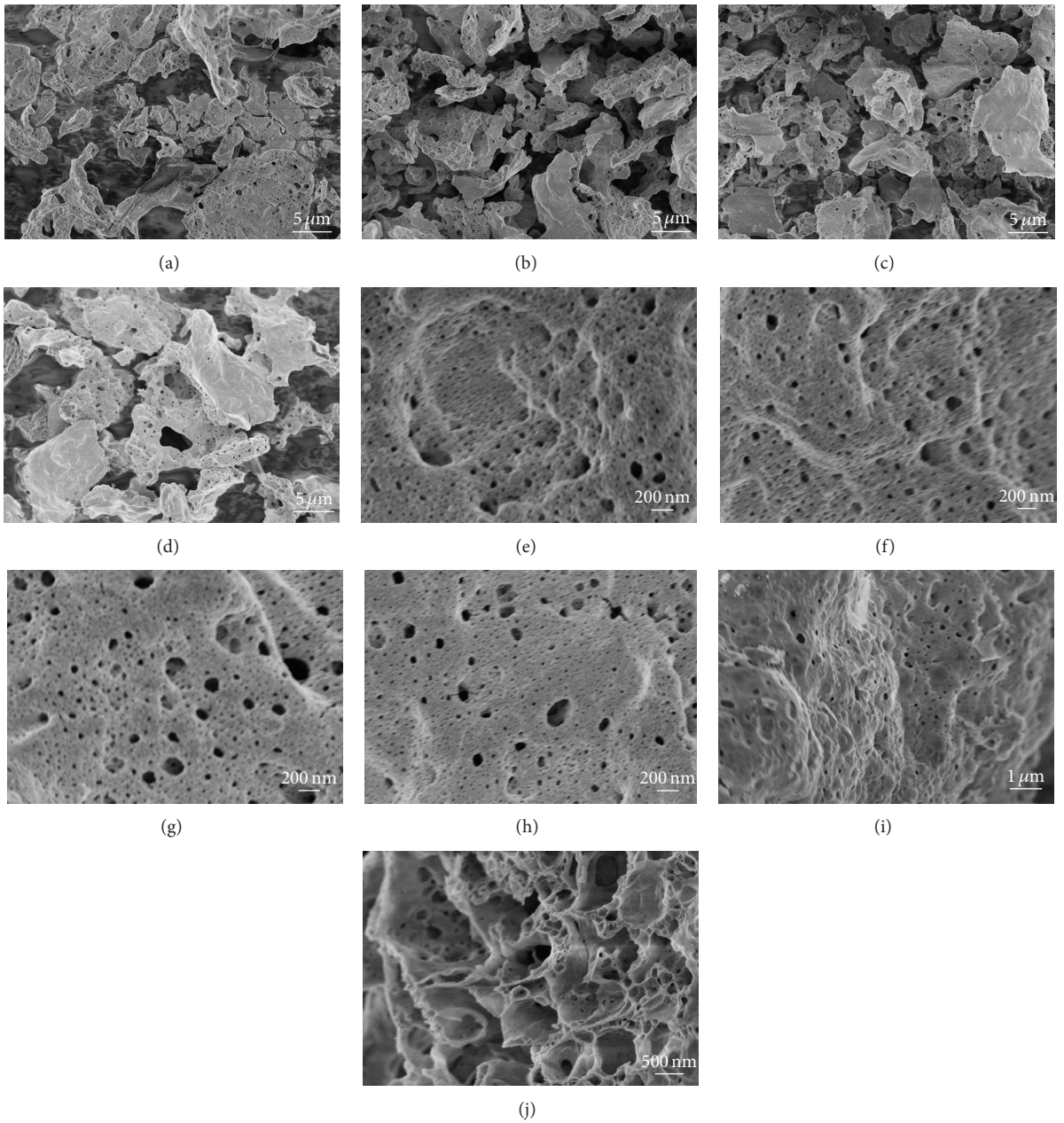

Figure 7: SEM images of Co_3O_4/CeO_2 photocatalysts with 5.0 wt.% Co_3O_4 calcined at 300°C (a and e), 400°C (b and f), 500°C (c and g), 600°C (d and h), and CeO_2 (i and j).

to 5 wt.%, the methanol yield increased from 0.68 to 1.52 μmol·g^{-1}·h^{-1} and the ethanol yield increased from 2.77 to 4.75 μmol·g^{-1}·h^{-1}. Further increasing the Co_3O_4 loading (>5 wt.%) leads to the decrease of the methanol and ethanol yields because of the significant decrease of the crystallization degree of CeO_2 shown in Figure 2. Photocatalytic activities of the sample with 5 wt.% Co_3O_4 were tested in different solutions. It is obvious that solution containing 0.1 M Na_2CO_3 and 0.1 M Na_2SO_3 has the best performance among (0.1 M Na_2CO_3 + 0.1 M Na_2SO_3), (0.1 M NaOH + 0.1 M Na_2SO_3), and (0.1 M Na_2CO_3 + 0.1M Na_2S), which indicates that extra carbon source (CO_3^{2-}) and better sacrifice reagent (SO_3^{2-}) can greatly enhance the photocatalytic activities for methanol and ethanol generation as shown in Table 2.

3.2. Effects of Calcination Temperature on the Photocatalytic Activity. Calcination temperature also affects the surface structures of catalysts. The samples with 5 wt.% of Co_3O_4 loading were calcined at 300°C, 400°C, and 500°C, respectively. As shown in Table 3, the specific surface area decreases with the increase of calcination temperature. And the pore diameter distribution becomes uneven when catalyst

Table 3: Characteristic of Co_3O_4/CeO_2 catalysts with 5 wt.% Co_3O_4 doping at different calcination temperatures.

Calcination temperature (°C)	BET surface area (m^2/g)	Average pore diameter (nm)	Total pore volume (cm^3g^{-1})	The crystallite size of CeO_2 (nm)
300	41.16	10.61	0.11	37.5
400	38.28	10.19	0.10	35.4
500	30.88	15.13	0.12	41.8

Table 4: Atomic compositions (%) measured from the O 1s, Ce 3d, and Co 3s spectra of CeO_2 and 5 wt.% Co_3O_4/CeO_2 samples at different calcination temperatures.

Calcination temperature (°C)	Atomic compositions (%)				Ce(III) : Ce(IV)
	O	Ce		Co	
		Ce(III)	Ce(IV)		
400 (CeO_2)	65.9	5.5	28.5	—	0.19
300	52.7	3.7	32.0	11.5	0.12
400	54.1	5.6	28.4	11.8	0.20
500	55.8	6.5	25.9	11.7	0.25

calcined at 500°C. Pore diameter bigger than 984 nm can be found from Figure 6, which indicates that the particle was melted and the pore collapsed.

Figure 7 shows the SEM images of the 5.0 wt.% Co_3O_4/CeO_2 catalysts prepared by calcining the spontaneous combusted precursor at temperatures of 300 to 600°C when CeO_2 calcined at 400°C. The shape of CeO_2 particle becomes very irregular. However, more pores can be seen on the surface of the CeO_2 particles (Figures 7(i) and 7(j)) compared to those of the Co_3O_4/CeO_2 catalysts (Figures 7(a)–7(h)). It can explain why the CeO_2 has larger surface area than the other samples. The particle size of the Co_3O_4/CeO_2 catalysts, however, increased greatly with the calcination temperature higher than 400°C, as shown in Figures 7(c) and 7(d). However, the particles of the sample calcined at 300°C are more irregular and the pores on the surface are bigger than those of the sample calcined at 400°C, which is in good correspondence to BET analysis results.

In Figure 3, XRD peaks for Co_3O_4 of Co_3O_4/CeO_2 catalysts are absent, however, the peaks appear when the calcination temperature is higher than 400°C as shown in Figure 8. And the CeO_2 crystallite size of catalysts was estimated by using the Scherrer equation, and the order is 500 (41.8 nm) > 300 (37.5 nm) > 400 (35.4 nm) as shown in Table 3. The diffraction peak at 48.6° corresponding to hexagonal Co-Ce-O phase (JCPDS file 65-5917) [36] becomes stronger with increase of calcination temperature, which suggests that the treatment by combustion method strengthens the Co-Ce interaction and the calcination temperature improves the crystallization structure of catalysts. Thus, the CeO_2 crystallite size is getting smaller under calcination temperature of 400°C than under 300°C. And the enlarged size of CeO_2 crystallite under 500°C is caused by sintering of particles which is in line with the SEM.

In order to determine the amount of Ce(III) in cerium oxides, the deconvolution method of the Ce3d

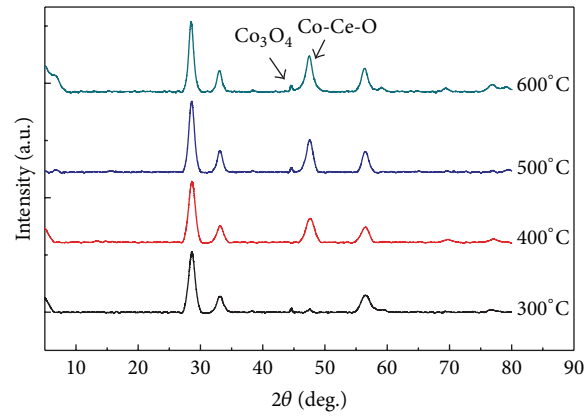

Figure 8: XRD pattern of Co_3O_4/CeO_2 photocatalysts under different calcination temperature.

features [34, 37] has been used. The amounts of Ce(III) and Ce(IV) were calculated from the components of the Ce 3d core level using the following equations [37]:

$$\text{Ce (III)} = v_0 + v' + u_0 + u' \quad (1)$$

$$\text{Ce (IV)} = v + v'' + v''' + u + u'' + u''' \quad (2)$$

$$\%\text{Ce (III)} = \left[\frac{\text{Ce (III)}}{(\text{Ce (III)} + \text{Ce (IV)})}\right] \times 100. \quad (3)$$

The calculated result shows that the amount of Ce(III) increases from 3.7% to 6.5%, the amount of Ce(IV) decreases from 32.0% to 25.9%, and the ratio of Ce(III) to Ce(IV) increases with the calcination temperature increase from 300°C to 500°C. These may be attributed to the reduction of carbon species which come from pyrolysis of residual glycine. The ratios of O to Ce atoms in CeO_2 and Ce_2O_3 lattice

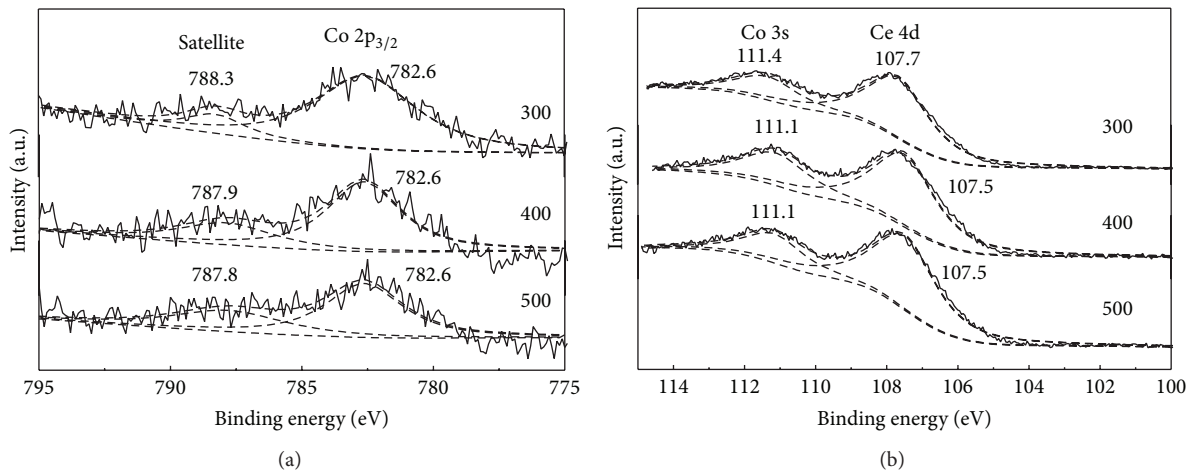

FIGURE 9: XPS spectra of (a) the Co 2p region and (b) the Co 3s-Ce 4d region for 5 wt.% Co_3O_4/CeO_2 prepared by calcining the spontaneous combusted precursor at temperatures 300°C, 400°C, and 500°C.

are 2 and 1.5, respectively. The measured results (Table 4) suggest that the oxygen amount on the surface of particles meets stoichiometric ratio with Ce(IV) and Ce(III) for the CeO_2 sample; however, it is far from sufficient for the Co-doped samples, which means that oxygen vacancies can be significantly formed on the surface of CeO_2 crystallite after cobalt is doped. Thus, the catalytic activity can be largely enhanced [38]. Among the Co-doped samples, the percentages of cobalt on surface of particle are almost constant, which indicates that the amount of oxygen vacancies decreases with the increase of calcination temperature. It is attributed to reduction of Co species on the surface during the generation of hexagonal Co-Ce-O phase [36].

Figure 9(a) shows the XPS spectra for Co 2p in 5 wt.% Co_3O_4/CeO_2 prepared by calcining the spontaneous combusted precursor at temperatures form 300°C to 500°C. The doublet peaks, corresponding to Co $2p_{3/2}$ and a satellite peak, for all the samples, were found at 788.0 ± 0.3 and 782.6 eV in Co 2p scanning pattern, which indicates the generation of Co_3O_4 on the surface of catalysts, which is in line with XRD analysis (Figure 8). Other researchers have reported that the satellite peak is absent in the diamagnetic Co^{3+} compound [39, 40]; however, it grows along with the increase of calcination temperature, which indicates the transformation of Co^{3+} to Co^{2+} species [41]. Whereas the binding energies of Co $2p_{3/2}$ and the satellite peak are slightly higher than the reported binding energies at ~780.0 and ~786.0 eV [41–43], respectively, this shift toward higher energies may be caused by the conjunction with Ce orbits. Binding energies of Co 3s and Ce 4d have been shown in Figure 9(b) to present the connection between Co and Ce orbits. Binding energy of Co 3s shifts toward higher energy from 110.9 (handbook [44]) to 111.4 or 111.1 eV, while binding energy of Ce 4d shifts toward lower energy from 110.0 (handbook [44]) to 107.7 or 107.5 eV, which suggests the formation of a kind of conjunction structure, and this structure becomes stable after calcining at temperature higher than 400°C.

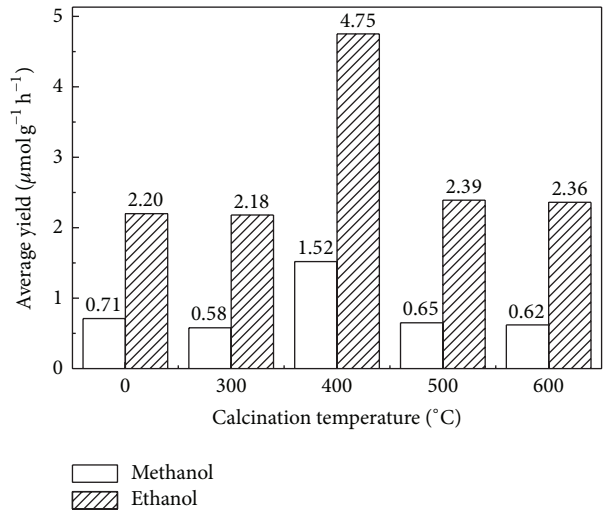

FIGURE 10: Photocatalytic activities of 5 wt.% Co_3O_4/CeO_2 under different calcination temperature (the sample without calcination is denoted as "0").

Figure 10 shows that catalysts calcined at 400°C have highest methanol and ethanol yield among all, which can be well explained by the BET and SEM analysis. The order of the photocatalytic activities arranged as the calcination temperature is 400 > 500 ≈ 600 > 300 > CeO_2, which is in line with that of XPS quantitative analysis.

3.3. Separation of Electron-Hole Pairs on Co_3O_4/CeO_2 Catalysts. The separation efficiency of electron-hole pairs of the composite photocatalyst is always the key factor to enhance the photocatalytic activity [26], which is mainly resulting from the addiction of cocatalyst. Ce^{3+} species formed on the surface of the composite might contribute to the separation of electron-hole pairs thus enhancing the photocatalytic

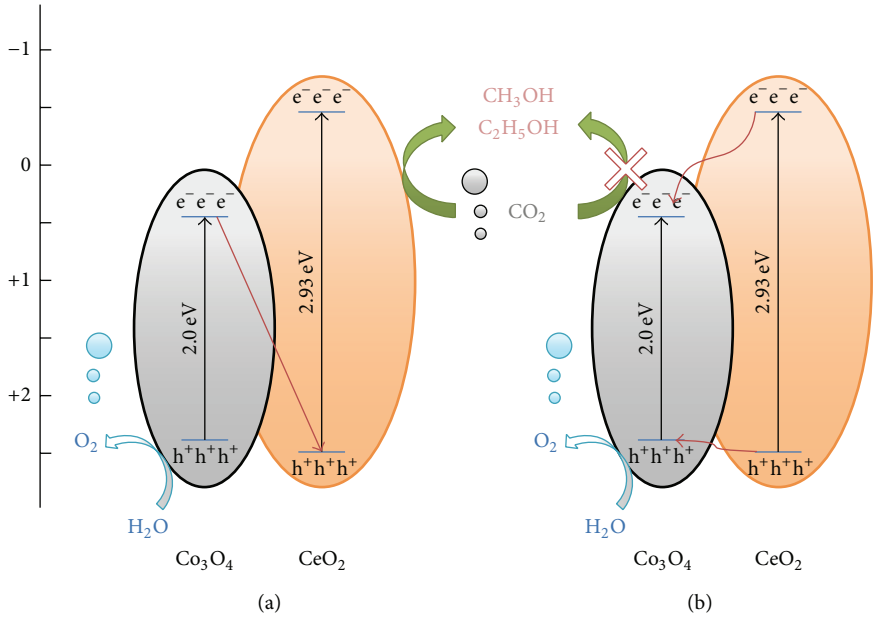

FIGURE 11: The scheme of photocatalytic reduction of carbon dioxide with water to methanol and ethanol.

activity [45] and further evidences will be discussed later. And doping Co_3O_4 can contribute to enhancing the visible absorption and it plays a role as a kind of cocatalyst to increase methanol and ethanol yields of photocatalytic reaction.

Two widely used equations for band edge calculation are showed below:

$$E_{CB} = \chi - E_c - \frac{1}{2}E_g$$
$$E_{VB} = E_g + E_{CB}. \quad (4)$$

E_{CB} is the conduction band edge of a semiconductor at the point of zero charge. χ is the absolute electronegativity of the semiconductor, expressed as the geometric mean of the absolute electronegativity of the constituent atoms, which is defined as the arithmetic mean of the atomic electron affinity and the first ionization energy. E_c is the energy of free electrons on the hydrogen scale (~4.5 eV). E_g is the band gap of the semiconductor [46, 47]. χ values for Co_3O_4 and CeO_2 are 5.93 and 5.53 eV, respectively. So the E_{CB} of Co_3O_4 and CeO_2 are calculated to be +0.43 and −0.44 eV, respectively, and the E_{VB} of Co_3O_4 and CeO_2 are estimated to be +2.43 and +2.49 eV, respectively. These results are close to those of the reported references [20, 30]. Figure 11(a) shows an assumption which was made to explain the separation of electron-hole pairs of Co_3O_4/CeO_2 catalysts. Photoelectron on the surface of Co_3O_4 transfers to the CeO_2 to avoid recombining to holes, which may also partly trap in the holes on CeO_2 and tend to reduce the recombination of electron-hole pairs on CeO_2. It works like a Z-scheme reaction. However, if the separation of electron-hole pairs works as p-n heterojunction, no methanol and ethanol would be produced because the conduction band potential of Co_3O_4 is too positive to reduce carbon dioxide (Figure 11(b)).

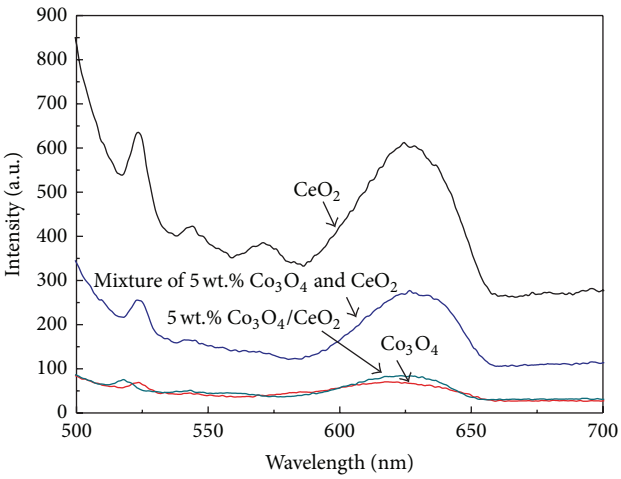

FIGURE 12: Photoluminescence spectra of CeO_2, 5 wt.% Co_3O_4 and CeO_2 mixture, and 5 wt.% Co_3O_4/CeO_2 and Co_3O_4.

In order to confirm that the enhancement of photocatalytic activity is due to charge transfer between Co_3O_4 and CeO_2, PL measurements were carried out. Figure 12 shows the spectra of CeO_2, Co_3O_4, 5 wt.% Co_3O_4/CeO_2, and mixture of 5 wt.% Co_3O_4 and CeO_2 while the 5 wt.% Co_3O_4/CeO_2 sample was prepared as a reference sample. The excitation wavelength was 425 nm. CeO_2 sample has a strong PL emission at about 630 nm, which indicates rapid recombination of electrons and holes. The other samples have a PL peak at the same position with a peak intensity order of CeO_2 > mixture > 5 wt.% Co_3O_4/CeO_2 ≈ Co_3O_4. The weak PL intensity of 5 wt.% Co_3O_4 and CeO_2 mixture could be attributed to the decrease of CeO_2 content. Although the sample contains only 5 wt.% of Co_3O_4, it has similar PL

peak intensity and shape to Co_3O_4. It suggests that Co_3O_4 can remarkably reduce the recombination of electrons and holes, and the charge transfer between Co_3O_4 and its carrier CeO_2 does exist, in which the result is in line with the XPS measurement (Figure 9(b)).

4. Conclusions

The Co_3O_4/CeO_2 photocatalysts with mesoporous structure were synthesized by glycine-nitrate combustion method to improve photocatalytic activity of carbon dioxide reduction. The experimental results indicate that the modification of Co_3O_4 can not only decrease the specific surface area and pore diameter but also greatly increase the visible light absorbance and the photocatalytic activity of CeO_2. The Co_3O_4/CeO_2 photocatalysts with 5 wt.% of Co_3O_4 loading calcined at 400°C were found to be the best catalysts for carbon dioxide reduction in 0.1 M Na_2CO_3 + 0.1 M Na_2SO_3 solution. The largest average yields of methanol and ethanol were 1.52 and 4.75 $\mu mol \cdot g^{-1} \cdot h^{-1}$, respectively. Furthermore, doping Co_3O_4 on the surface of CeO_2 can help to promote separation of electron-hole and electron transfer between these two semiconductors. PL spectra revealed that Z-scheme charge transfer, one of the factors to enhance photocatalytic activity, occurred on the surface of Co_3O_4/CeO_2 catalysts under visible light irradiation.

Conflict of Interests

The authors declare that there is no conflict of interests regarding the publication of this paper.

Acknowledgments

The authors gratefully acknowledge the financial support of CAS Renewable Energy Key Lab., Guangdong Science and Technology Project (2013B050800007), and Guangzhou Science and Technology Project (2013J4500027).

References

[1] Y. Izumi, "Recent advances in the photocatalytic conversion of carbon dioxide to fuels with water and/or hydrogen using solar energy and beyond," *Coordination Chemistry Reviews*, vol. 257, no. 1, pp. 171–186, 2013.

[2] G. Liu, N. Hoivik, K. Wang, and H. Jakobsen, "Engineering TiO_2 nanomaterials for CO_2 conversion/solar fuels," *Solar Energy Materials and Solar Cells*, vol. 105, pp. 53–68, 2012.

[3] J. C. S. Wu and H.-M. Lin, "Photo reduction of CO_2 to methanol via TiO_2 photocatalyst," *International Journal of Photoenergy*, vol. 7, no. 3, pp. 115–119, 2005.

[4] X. Li, H. Liu, D. Luo et al., "Adsorption of CO_2 on heterostructure $CdS(Bi_2S_3)/TiO_2$ nanotube photocatalysts and their photocatalytic activities in the reduction of CO_2 to methanol under visible light irradiation," *Chemical Engineering Journal*, vol. 180, pp. 151–158, 2012.

[5] X. Li, J. T. Chen, H. L. Li et al., "Photoreduction of CO_2 to methanol over Bi_2S_3/CdS photocatalyst under visible light irradiation," *Journal of Natural Gas Chemistry*, vol. 20, no. 4, pp. 413–417, 2011.

[6] H. Li, Y. Lei, Y. Huang et al., "Photocatalytic reduction of carbon dioxide to methanol by Cu_2O/SiC nanocrystallite under visible light irradiation," *Journal of Natural Gas Chemistry*, vol. 20, no. 2, pp. 145–150, 2011.

[7] J. Mao, T. Peng, X. Zhang, K. Li, L. Ye, and L. Zan, "Effect of graphitic carbon nitride microstructures on the activity and selectivity of photocatalytic CO_2 reduction under visible light," *Catalysis Science & Technology*, vol. 3, no. 5, pp. 1253–1260, 2013.

[8] K. Maeda, K. Sekizawa, and O. Ishitani, "A polymeric-semiconductor-metal-complex hybrid photocatalyst for visible-light CO_2 reduction," *Chemical Communications*, vol. 49, no. 86, pp. 10127–10129, 2013.

[9] X.-J. Lv, W.-F. Fu, C.-Y. Hu, Y. Chen, and W.-B. Zhou, "Photocatalytic reduction of CO_2 with H_2O over a graphene-modified NiO_x-Ta_2O_5 composite photocatalyst: coupling yields of methanol and hydrogen," *RSC Advances*, vol. 3, no. 6, pp. 1753–1757, 2013.

[10] H.-C. Hsu, I. Shown, H.-Y. Wei et al., "Graphene oxide as a promising photocatalyst for CO_2 to methanol conversion," *Nanoscale*, vol. 5, no. 1, pp. 262–268, 2013.

[11] S. Hu, F. Zhou, L. Wang, and J. Zhang, "Preparation of Cu_2O/CeO_2 heterojunction photocatalyst for the degradation of Acid Orange 7 under visible light irradiation," *Catalysis Communications*, vol. 12, no. 9, pp. 794–797, 2011.

[12] T. Cai, Y. Liao, Z. Peng, Y. Long, Z. Wei, and Q. Deng, "Photocatalytic performance of TiO_2 catalysts modified by $H_3PW_{12}O_{40}$, ZrO_2 and CeO_2," *Journal of Environmental Sciences*, vol. 21, no. 7, pp. 997–1004, 2009.

[13] Y. Wang, B. Li, C. Zhang et al., "Ordered mesoporous CeO_2-TiO_2 composites: highly efficient photocatalysts for the reduction of CO_2 with H_2O under simulated solar irradiation," *Applied Catalysis B: Environmental*, vol. 130, pp. 277–284, 2013.

[14] L. Li and B. Yan, "CeO_2-Bi_2O_3 nanocomposite: two step synthesis, microstructure and photocatalytic activity," *Journal of Non-Crystalline Solids*, vol. 355, no. 13, pp. 776–779, 2009.

[15] F. Zhang, A. Yamakata, K. Maeda et al., "Cobalt-modified porous single-crystalline $LaTiO_2N$ for highly efficient water oxidation under visible light," *Journal of the American Chemical Society*, vol. 134, no. 20, pp. 8348–8351, 2012.

[16] S. S. K. Ma, K. Maeda, T. Hisatomi, M. Tabata, A. Kudo, and K. Domen, "A redox-mediator-free solar-driven Z-scheme water-splitting system consisting of modified Ta_3N_5 as an oxygen-evolution photocatalyst," *Chemistry: A European Journal*, vol. 19, no. 23, pp. 7480–7486, 2013.

[17] J. del Pilar-Albaladejo and P. K. Dutta, "Topotactic transformation of zeolite supported cobalt(II) hydroxide to oxide and comparison of photocatalytic oxygen evolution," *ACS Catalysis*, vol. 4, no. 1, pp. 9–15, 2014.

[18] H. Ye, H. S. Park, and A. J. Bard, "Screening of electrocatalysts for photoelectrochemical water oxidation on W-doped $BiVO_4$ photocatalysts by scanning electrochemical microscopy," *The Journal of Physical Chemistry C*, vol. 115, no. 25, pp. 12464–12470, 2011.

[19] P. A. Mangrulkar, M. M. Joshi, S. N. Tijare, V. Polshettiwar, N. K. Labhsetwar, and S. S. Rayalu, "Nano cobalt oxides for photocatalytic hydrogen production," *International Journal of Hydrogen Energy*, vol. 37, no. 13, pp. 10462–10466, 2012.

[20] A. K. Chakraborty, M. Shanjeda Akter, M. Ahsanul Haque, G. M. Arifuzzaman Khan, and M. Shamsul Alam, "Synthesis of Co_3O_4/WO_3 nanoheterojunction photocatalyst for the decomposition of organic pollutants under visible light irradiation," *Journal of Cluster Science*, vol. 24, no. 3, pp. 701–713, 2013.

[21] S.-H. Hsieh, G.-J. Lee, C.-Y. Chen et al., "Hydrothermal synthesis of mesoporous Bi_2O_3/Co_3O_4 microsphere and photocatalytic degradation of orange II dyes by visible light," *Topics in Catalysis*, vol. 56, no. 9-10, pp. 623–629, 2013.

[22] H. Sun, S. Liu, G. Zhou, H. M. Ang, M. O. Tadé, and S. Wang, "Reduced graphene oxide for catalytic oxidation of aqueous organic pollutants," *ACS Applied Materials & Interfaces*, vol. 4, no. 10, pp. 5466–5471, 2012.

[23] M. Long, W. Cai, J. Cai, B. Zhou, X. Chai, and Y. Wu, "Efficient photocatalytic degradation of phenol over $Co_3O_4/BiVO_4$ composite under visible light irradiation," *The Journal of Physical Chemistry B*, vol. 110, no. 41, pp. 20211–20216, 2006.

[24] K. Kondo, N. Murakami, C. Ye, T. Tsubota, and T. Ohno, "Development of highly efficient sulfur-doped TiO_2 photocatalysts hybridized with graphitic carbon nitride," *Applied Catalysis B: Environmental*, vol. 142-143, pp. 362–367, 2013.

[25] H. Katsumata, Y. Tachi, T. Suzuki, and S. Kaneco, "Z-scheme photocatalytic hydrogen production over WO_3/g-C_3N_4 composite photocatalysts," *RSC Advances*, vol. 4, no. 41, pp. 21405–21409, 2014.

[26] Y. M. He, L. H. Zhang, X. X. Wang et al., "Enhanced photodegradation activity of methyl orange over Z-scheme type MoO_3-g-C_3N_4 composite under visible light irradiation," *RSC Advances*, vol. 4, no. 26, pp. 13610–13619, 2014.

[27] S. F. Chen, Y. F. Hu, L. Ji, X. L. Jiang, and X. L. Fu, "Preparation and characterization of direct Z-scheme photocatalyst $Bi_2O_3/NaNbO_3$ and its reaction mechanism," *Applied Surface Science*, vol. 292, pp. 357–366, 2014.

[28] S. Hajarpour, K. Gheisari, and A. Honarbakhsh Raouf, "Characterization of nanocrystalline $Mg_{0.6}Zn_{0.4}Fe_2O_4$ soft ferrites synthesized by glycine-nitrate combustion process," *Journal of Magnetism and Magnetic Materials*, vol. 329, pp. 165–169, 2013.

[29] C.-F. Yan, H. Chen, R.-R. Hu et al., "Synthesis of mesoporous Co–Ce oxides catalysts by glycine-nitrate combustion approach for CO preferential oxidation reaction in excess H_2," *International Journal of Hydrogen Energy*, vol. 39, no. 32, pp. 18695–18701, 2014.

[30] L. Matějová, K. Kočí, M. Reli et al., "Preparation, characterization and photocatalytic properties of cerium doped TiO_2: on the effect of Ce loading on the photocatalytic reduction of carbon dioxide," *Applied Catalysis B: Environmental*, vol. 152-153, pp. 172–183, 2014.

[31] N. Zhang, S. Liu, X. Fu, and Y.-J. Xu, "A simple strategy for fabrication of 'plum-pudding' type Pd@CeO_2 semiconductor nanocomposite as a visible-light-driven photocatalyst for selective oxidation," *The Journal of Physical Chemistry C*, vol. 115, no. 46, pp. 22901–22909, 2011.

[32] S. Sharma, P. Singh, and M. S. Hegde, "Electrocatalysis and redox behavior of Pt^{2+} ion in CeO_2 and $Ce_{0.85}Ti_{0.15}O_2$: XPS evidence of participation of lattice oxygen for high activity," *Journal of Solid State Electrochemistry*, vol. 15, no. 10, pp. 2185–2197, 2011.

[33] E. Abiaad, R. Bechara, J. Grimblot, and A. Aboukais, "Preparation and characterization of CeO_2 under an oxidizing atmosphere—thermal-analysis, Xps, and Epr study," *Chemistry of Materials*, vol. 5, pp. 793–797, 1993.

[34] E. Beche, G. Peraudeau, V. Flaud, and D. Perarnau, "An XPS investigation of $(La_2O_3)_{1-x}$ $(CeO_2)_{2x}$ $(ZrO_2)_2$ compounds," *Surface and Interface Analysis*, vol. 44, no. 8, pp. 1045–1050, 2012.

[35] H. Chen, S. W. Lee, T. H. Kim, and B. Y. Hur, "Photocatalytic decomposition of benzene with plasma sprayed TiO_2-based coatings on foamed aluminum," *Journal of the European Ceramic Society*, vol. 26, no. 12, pp. 2231–2239, 2006.

[36] T. Bao, Z. Zhao, Y. Dai et al., "Supported Co_3O_4-CeO_2 catalysts on modified activated carbon for CO preferential oxidation in H_2-rich gases," *Applied Catalysis B: Environmental*, vol. 119-120, pp. 62–73, 2012.

[37] M. Romeo, K. Bak, E. Fallah, F. Le Normand, and L. Hilaire, "XPS study of the reduction of cerium dioxide," *Surface and Interface Analysis*, vol. 20, no. 6, pp. 508–512, 1993.

[38] A. Krishnan, T. S. Sreeremya, E. Murray, and S. Ghosh, "One-pot synthesis of ultra-small cerium oxide nanodots exhibiting multi-colored fluorescence," *Journal of Colloid and Interface Science*, vol. 389, no. 1, pp. 16–22, 2013.

[39] M. Kang, M. W. Song, and C. H. Lee, "Catalytic carbon monoxide oxidation over CoO_x/CeO_2 composite catalysts," *Applied Catalysis A: General*, vol. 251, no. 1, pp. 143–156, 2003.

[40] L. F. Liotta, G. Di Carlo, G. Pantaleo, A. M. Venezia, and G. Deganello, "Co_3O_4/CeO_2 composite oxides for methane emissions abatement: relationship between Co_3O_4-CeO_2 interaction and catalytic activity," *Applied Catalysis B: Environmental*, vol. 66, no. 3-4, pp. 217–227, 2006.

[41] L. E. Gómez, I. S. Tiscornia, A. V. Boix, and E. E. Miró, "CO preferential oxidation on cordierite monoliths coated with Co/CeO_2 catalysts," *International Journal of Hydrogen Energy*, vol. 37, no. 19, pp. 14812–14819, 2012.

[42] L. Óvári, S. Krick Calderon, Y. Lykhach et al., "Near ambient pressure XPS investigation of the interaction of ethanol with Co/CeO_2(1 1 1)," *Journal of Catalysis*, vol. 307, pp. 132–139, 2013.

[43] H. Idriss, C. Diagne, J. P. Hindermann, A. Kiennemann, and M. A. Barteau, "Reactions of acetaldehyde on CeO_2 and CeO_2-supported catalysts," *Journal of Catalysis*, vol. 155, no. 2, pp. 219–237, 1995.

[44] B. V. Crist, *Handbooks of Monochromatic XPS Spectra. The Elements and Native Oxides*, XPS International, Mountain View, Calif, USA, 1999.

[45] M. M. Khan, S. A. Ansari, D. Pradhan, D. H. Han, J. Lee, and M. H. Cho, "Defect-induced band gap narrowed CeO_2 nanostructures for visible light activities," *Industrial & Engineering Chemistry Research*, vol. 53, pp. 9754–9763, 2014.

[46] S. F. Chen, Y. F. Hu, L. Ji, X. Jiang, and X. Fu, "Preparation and characterization of direct Z-scheme photocatalyst $Bi_2O_3/NaNbO_3$ and its reaction mechanism," *Applied Surface Science*, vol. 292, pp. 357–366, 2014.

[47] S. Chen, Y. Hu, S. Meng, and X. Fu, "Study on the separation mechanisms of photogenerated electrons and holes for composite photocatalysts g-C_3N_4-WO_3," *Applied Catalysis B: Environmental*, vol. 150-151, pp. 564–573, 2014.